Chain-Length Dependence of Diblock Copolymer Micellization Kinetics Studied by Stopped-Flow pH-Jump

Jingyan Zhang,[†,‡] Jian Xu,[†] and Shiyong Liu*[,†]

Key Laboratory of Soft Matter Chemistry, Department of Polymer Science and Engineering, Hefei National Laboratory for Physical Sciences at the Microscale, University of Science and Technology of China, Hefei, Anhui 230026, China, and School of Materials and Chemical Engineering, Anhui University of Architecture, Hefei, Anhui 230022, China

Received: April 28, 2008; Revised Manuscript Received: July 1, 2008

A series of well-defined poly(ethylene oxide)-*b*-poly(2-(diethylamino)ethyl methacrylate) (PEO-*b*-PDEA) diblock copolymers containing PEO block of identical chain length and PDEA block with varying degrees of polymerization (DP, in the range of 32−154) were prepared via atom transfer radical polymerization (ATRP) employing a PEO-based macroinitiator (DP = 113). Upon a pH-jump from 3 to 12 under highly efficient stopped-flow mixing conditions, PEO-*b*-PDEA copolymers spontaneously form spherical micelles of increasing sizes and aggregation numbers (N_{agg}) with increasing PDEA chain lengths. Stopped-flow light scattering technique was used to probe the pH-induced micellization kinetics of PEO-*b*-PDEA copolymers, aiming to elucidate the PDEA chain-length effects on the unimer-to-micelle transition process. Upon a stopped-flow pH-jump from 3 to 12, the obtained dynamic traces can be well-fitted with double exponential functions. The calculated fast and slow characteristic relaxation times (τ_1 and τ_2) can be ascribed to the formation of quasi-equilibrium micelles (fast process) and subsequent relaxation into final equilibrium micelles (slow process), respectively. For PEO_{113}-*b*-$PDEA_{32}$ and PEO_{113}-*b*-$PDEA_{61}$, τ_2 is almost independent of polymer concentrations, suggesting that the relaxation from quasi-equilibrium micelles into final equilibrium micelles mainly proceeds via insertion/expulsion of unimer chains. Upon increasing the DP of pH-responsive PDEA block to 89, 117, and 154, the obtained slow relaxation time, τ_2, tends to decrease with increasing polymer concentrations, suggesting that the slow process is dominated by the micelle fusion/fission mechanism. The apparent activation energy (E_a) associated with τ_2 has also been determined from temperature-dependent micellization kinetics for five PEO-*b*-PDEA copolymers. It was found that during micellization, copolymers with longer PDEA blocks exhibit much lower E_a compared to those with shorter blocks. Thus, we observed experimentally for the first time that increasing the hydrophobic block length in double hydrophilic block copolymers (DHBCs) can transform the mechanism of the slow process from unimer insertion/expulsion to micelle fusion/fission.

Introduction

Double hydrophilic block copolymers (DHBCs)[1−10] have received ever-increasing interest in the past decade due to their promising applications in diverse fields such as drug delivery, gene therapy, interface mediators, soft actuators/valves, and catalysis.[11−18] Particularly, DHBC containing a biocompatible PEO block[19−23] and a pH-responsive block has been extensively investigated due to that pH variation can be readily realized both in vitro and in vivo.[24] The first example of PEO-containing pH-responsive DHBC, poly(ethylene oxide)-*b*-poly(2-vinyl pyridine) (PEO-*b*-P2VP), was reported by Martin et al.[25] Armes and co-workers[26−30] later reported more sophisticated examples of DHBCs containing the pH-responsive poly(2-(diethylamino)ethyl methacrylate) (PDEA) building block. Some of them even exhibited "schizophrenic" micellization character, forming two or more types of structurally "inverted" micelles in aqueous solution via judicious manipulation of solution pH, temperature, and salt concentration.[31−33]

Concerning micellization properties of the simplest system, PEO-*b*-PDEA, Lee et al.[34] characterized the structures of spherical micelles formed from PEO-*b*-PDEA in dilute aqueous solution as a function of pH and ionic strengths. Tan et al.[35] investigated the aggregation behavior of biotinylated and nonbiotinylated PEO-*b*-PDEA copolymers in aqueous solution at varying pH and ionic strengths, aiming to explore their potential biomedical applications. Recently, Adams et al.[19] synthesized a series of PEO-*b*-PDEA copolymers with relatively high polydispersity (1.36 < PDI < 1.96) and investigated their self-assembly behavior in dilute solution. Upon intentionally increasing the sample polydispersity by adjusting the polymerization conditions, they obtained a variety of self-assembled structures ranging from spherical micelles, wormlike micelles, to vesicles, which is dependent on the relative chain-length ratios.

Previous reports of the self-assembly of PEO-*b*-PDEA copolymers mainly focused on the characterization of their final equilibrium structures by various techniques such as laser light scattering (LLS), small angle neutron scattering (SANS), and transmission electron microscopy (TEM).[19,34−36] On the other hand, much less has been explored concerning the unimer-to-micelle transition kinetics, which is expected to exhibit great significance for related technological processes in practical applications. It should be noted that theoretical considerations of the micellization kinetics of diblock copolymers have been

* To whom correspondence should be addressed. E-mail: sliu@ustc.edu.cn.
† University of Science and Technology of China.
‡ Anhui University of Architecture.

10.1021/jp803700n CCC: $40.75
Published on Web 08/15/2008

proposed by Wang et al.,[37] Dormidontova and co-workers,[38−40] and Nyrkova and Semenov.[41,42] However, a general consensus has not been reached yet.

In the past few years, we have investigated the kinetics of unimer-to-micelle transition and structural inversion between different types of micelles for a series of stimuli-responsive DHBCs by employing the stopped-flow technique. Upon stopped-flow pH-, temperature-, and salt-jump, the time-dependent scattered intensity accompanied with the evolution of micelles can be obtained. For poly(glycerol monomethacrylate)-*b*-poly(2-(dimethylamino)ethyl methacrylate)-*b*-poly(2-(diethylamino)ethyl methacrylate) (PGMA-*b*-PDMA-*b*-PDEA),[43] the micellization kinetics was analyzed in the context of Dormidontova model. Upon jumping the solution pH from 4 to 12, the micellization proceeded via two successive processes. The initial fast process (τ_1) is associated with the formation of quasi-equilibrium micelles, and the subsequent slow process (τ_2) is attributed to micelle formation and breakup, approaching the final equilibrium state. τ_2 is almost independent of copolymer concentrations, indicating that the slow process proceeds mainly via the unimer insertion/expulsion mechanism. Recently, we further investigated the effects of added salts on the pH-induced micellization kinetics. It was found that at elevated salt concentrations, the slow process associated with τ_2 tends to proceed via the micelle fusion/fission mechanism.[44]

It is noteworthy that experimentally determining the block chain-length dependence of unimer-to-micelle transition kinetics should be very instructive.[40] The results can be directly compared to those deduced from theoretical considerations, which might lead to a clearer picture concerning the mechanism of micellization kinetics. In this work, we synthesized a series of well-defined PEO-*b*-PDEA diblock copolymers containing identical PEO block and pH-responsive PDEA block with varying degrees of polymerization (DP, in the range of 32−154) via atom transfer radical polymerization (ATRP) employing a PEO-based macroinitiator (DP = 113). Spherical micelles of increasing sizes can spontaneously form from PEO-*b*-PDEA copolymers with increasing PDEA block lengths upon a pH-jump from 3 to 12 under highly efficient stopped-flow mixing conditions. The pH-induced micellization kinetics of PEO-*b*-PDEA block copolymers has been systematically investigated so as to elucidate the effect of varying the PDEA chain length.

Experimental Section

Materials. 2-(Diethylamino)ethyl methacrylate (DEA, Aldrich) was vacuum-distilled from CaH_2 and stored at −20 °C prior to use. Copper(I) bromide (CuBr), 2,2′-bipyridine (bpy), 2-bromoisobutyryl bromide, and monohydroxy-capped poly(ethylene oxide) (PEO_{113}−OH, mean DP = 113, and M_w/M_n = 1.06) were obtained from Aldrich and used as received. PEO-based ATRP macroinitiator (PEO_{113}−Br) was synthesized by the reaction of PEO_{113}−OH with 2-bromoisobutyryl bromide according to literature procedures.[28] All other reagents were purchased from Sinopharm Chemical Reagent Co. Ltd. and used as received.

Sample Preparation. PEO-*b*-PDEA diblock copolymers were synthesized via ATRP using PEO_{113}−Br as the macroinitiator, and a typical procedure was as follows. A reaction flask with a magnetic stirrer and a rubber septum was charged with PEO_{113}−Br (3.60 g, 0.72 mmol), DEA (9.4 mL, 46.8 mmol), bpy (113 mg, 0.72 mmol), and 2-propanol (12 mL). The flask was degassed by three freeze−pump−thaw cycles, back-filled with N_2. CuBr (103 mg, 0.72 mmol) was added to start the polymerization at room temperature under the protection of N_2 flow. After 2 h, the reaction flask was quenched in liquid nitrogen, exposed to air, and diluted with 10 mL of 2-propanol. The reaction mixture was then passed through a silica gel column to remove the copper catalyst. After removing all the solvent on a rotary evaporator, the residues were dissolved in CH_2Cl_2 and precipitated into an excess of cold *n*-hexane (−70 °C) to remove residual monomers. After drying overnight in a vacuum oven at room temperature, colorless and viscous solids were obtained with a yield of ∼95%. The molecular weight and molecular weight distribution of PEO-*b*-PDEA diblock copolymer were determined by gel permeation chromatography (GPC) using tetrahydrofuran (THF) as the eluent: M_n = 16 500, M_w/M_n = 1.11. The DP of the PDEA block was determined to be 61 by ^{1}H NMR in $CDCl_3$, and the obtained polymer was denoted as PEO_{113}-*b*-$PDEA_{61}$. According to similar procedure, a series of PEO-*b*-PDEA copolymers with varying PDEA chain lengths were also synthesized, and their structural parameters are listed in Table 1.

TABLE 1: Molecular Parameters of PEO_{113}-*b*-$PDEA_m$ Double Hydrophilic Diblock Copolymers

entry	M_n[a]	M_w[a]	M_w/M_n[a]	*m*, $PDEA_m$[b]	f_{EO}[c]
PEO_{113}-*b*-$PDEA_{32}$	11 700	12 200	1.04	32	0.47
PEO_{113}-*b*-$PDEA_{61}$	16 500	18 300	1.11	61	0.32
PEO_{113}-*b*-$PDEA_{89}$	28 400	35 800	1.26	89	0.24
PEO_{113}-*b*-$PDEA_{117}$	29 600	36 400	1.23	117	0.20
PEO_{113}-*b*-$PDEA_{154}$	34 200	42 400	1.24	154	0.16

[a] Measured by GPC using THF as eluent. [b] Calculated from ^{1}H NMR. [c] Volume fraction of the PEO block calculated using ρ_{PEO} = 1.13 g/cm^3 and ρ_{PDEA} = 1.19 g/cm^3.

Self-Assembly via Stopped-Flow pH-Jump. PEO-*b*-PDEA copolymers were dissolved in water at pH 3 at a concentration of 4.0 g/L. Upon rapid mixing with NaOH solution on the stopped-flow device, the pH-jump from 3 to 12 can be realized in less than 1 ms. The colloidal dispersion at a final concentration of 2.0 g/L after the pH-jump was collected. It was then used for subsequent LLS and TEM analysis after further dilution.

Characterization. ***Nuclear Magnetic Resonance Spectroscopy.*** All ^{1}H NMR spectra were recorded in $CDCl_3$ at 25 °C on a Bruker AV300 NMR spectrometer (resonance frequency of 300 MHz for ^{1}H) operating in the Fourier transform mode.

Gel Permeation Chromatography. Molecular weights and molecular weight distributions were determined by GPC equipped with Waters 1515 pump and Waters 2414 differential refractive index detector (set at 30 °C). It used a series of three linear Styragel columns HT2, HT4, and HT5 at an oven temperature of 45 °C. The eluent was THF at a flow rate of 1.0 mL/min. A series of low-polydispersity poly(methyl mathacrylate) (PMMA) standards were employed for the GPC calibration.

Transmission Electron Microscopy. TEM observations were conducted on a Philips CM 120 electron microscope at an acceleration voltage of 100 kV. Samples for TEM observations were prepared by placing 10 μL of micellar solution on copper grids coated with thin films of Formvar and carbon successively. No staining was required.

Laser Light Scattering. A commercial spectrometer (ALV/DLS/SLS-5022F) equipped with a multitau digital time correlator (ALV5000) and a cylindrical 22 mW UNIPHASE He−Ne laser (λ_0 = 632 nm) as the light source was employed for dynamic LLS measurements. Scattered light was collected at a fixed angle of 90° for duration of ∼10 min. Distribution averages and particle size distributions were computed using cumulants analysis and CONTIN routines. All data were averaged over three measurements.

In static LLS, we can obtain the weight-average molar mass (M_w) and the z-average root-mean-square radius of gyration ($\langle R_g^2\rangle^{1/2}$ or written as $\langle R_g\rangle$) of polymer chains in a dilute solution from the angular dependence of the excess absolute scattering intensity, known as Rayleigh ratio $R_{vv}(q)$, as

$$\frac{KC}{R_{vv}(q)} \approx \frac{1}{M_w}\left(1 + \frac{1}{3}\langle R_g^2\rangle q^2\right) + 2A_2C \qquad (1)$$

where $K = 4\pi^2n^2(dn/dC)^2/(N_A\lambda_0^4)$ and $q = (4\pi n/\lambda_0)\sin(\theta/2)$ with N_A, dn/dC, n, and λ_0 being the Avogadro number, the specific refractive index increment, the solvent refractive index, and the wavelength of laser light in a vacuum, respectively; A_2 is the second virial coefficient. The specific refractive index increment was determined by a precise differential refractometer. Also note that in this study, the sample solution was so dilute (0.1 g/L) that the extrapolation of $C \rightarrow 0$ was not necessary, and the term $2A_2C$ in eq 1 can be neglected. Thus, the obtained M_w should be considered as apparent values, denoted as $M_{w,app}$.

Stopped-Flow with Light Scattering Detection. Stopped-flow studies were carried out using a Bio-Logic SFM300/S stopped-flow instrument. It is equipped with three 10 mL step-motor-driven syringes (S1, S2, and S3), which can be operated independently to carry out single- or double-mixing. The stopped-flow device is attached to a MOS-250 spectrometer; kinetic data were fitted using the Biokine program provided by Bio-Logic. For the light scattering detection at a scattering angle of 90°, both the excitation and emission wavelengths were adjusted to 335 nm with 10 nm slits. With the use of FC-08 or FC-15 flow cells, typical dead times are 1.1 and 2.6 ms, respectively.

Results and Discussion

Synthesis and Self-Assembly of PEO-*b*-PDEA Copolymers. The controlled radical polymerization of DEA monomer has been well-established, and a variety of PDEA-containing stimuli-responsive diblock and triblock copolymers were prepared.[19,28,34−36,45,46] Tan et al.[35] reported the synthesis of PEO-*b*-PDEA copolymers with or without a biotin terminal functionality via ATRP in water/methanol mixture, and the polydispersity was ∼1.3. Under different conditions, Adams et al.[19] intentionally prepared PEO-*b*-PDEA copolymers with relatively high polydispersities (1.36 < PDI < 1.96) via ATRP in 2-butanone at 80 °C and examined the effects of relative block lengths and polydispersity on the self-assembled morphology. It seems that the solvent polarity can dramatically affect the polymerization rate and PDI.[47,48] In the current study, we choose 2-propanol as the solvent, which has been proved to be an excellent solvent for DEA and 2-(dimethylamino)ethyl methacrylate (DMA) monomers;[49] moreover, the polymerization of DEA and DMA in 2-propanol can effectively eliminate side reactions such as transesterification, which might occur in methanol.[49] Table 1 lists the structural parameters of a series of PEO-*b*-PDEA copolymers with PDI in the range of 1.04−1.26.

Previous investigations suggested that the polydispersity of block copolymers can exhibit dramatic effects on the morphology of final aggregates.[50−52] Terreau et al.[51] studied the self-assembly of a series of polystyrene-*b*-poly(acrylic acid) (PS-*b*-PAA) diblock copolymers of increasing polydispersity for the PAA block. They found that at relatively high water content, the self-assembled morphology can range from spheres, rods, to vesicles depending on the PDI of PAA block. For a series of PEO-*b*-PDEA copolymers with relatively broad polydispersity, Adams et al.[19] observed the evolution of self-assembled morphology with the volume fraction of PEO block (f_{EO}), forming spherical micelles, rodlike micelles, and vesicles at high, intermediate, and low (<∼0.1) f_{EO} values, respectively.

TABLE 2: Dynamic and Static LLS Characterization of Micelles Prepared from PEO_{113}-*b*-$PDEA_m$ Diblock Copolymers via Stopped-Flow Mixing[a]

entry	$\langle R_h\rangle$ (nm)[b]	μ_2/Γ^2 [b]	$\langle R_c\rangle$ (nm)[c]	$M_{w,app}$ (g/mol)[d]	N_{agg}[e]	ρ (g/cm^3)[f]
PEO_{113}-*b*-$PDEA_{32}$	11	0.11	2	4.02×10^5	35	0.12
PEO_{113}-*b*-$PDEA_{61}$	13	0.09	4	7.76×10^5	43	0.14
PEO_{113}-*b*-$PDEA_{89}$	14	0.07	5	1.18×10^6	44	0.17
PEO_{113}-*b*-$PDEA_{117}$	16	0.12	7	1.86×10^6	57	0.18
PEO_{113}-*b*-$PDEA_{154}$	19	0.14	10	3.63×10^6	87	0.17

[a] The micellar solution was prepared via pH-jump from 3 to 12 upon stopped-flow mixing of unimer solutions at pH 3 with NaOH solution. [b] Determined by dynamic LLS at a scattering angle of 90° and a polymer concentration of 2.0 g/L; the estimated error associated with each value was ±2 nm. [c] The average radii of insoluble PDEA cores, $\langle R_c\rangle$, were estimated from the scaling law proposed by Wu and Gao (ref 55), assuming that PEO corona of all PDEA-core micelles occupy the same brush thickness. [d] The apparent molar masses, $M_{w,app}$, of micelles were determined by static LLS at a concentration of 0.1 g/L. [e] Calculated as $N_{agg} = M_{w,app}/M_w$, where M_w is the weight-average molecular weight of PEO_{113}-*b*-$PDEA_m$ diblock copolymers. [f] Calculated as $\rho = M_{w,app}/(4\pi/3N_A\langle R_h\rangle^3)$, where N_A is the Avogadro number.

In the current study, a series of relatively near-monodisperse PEO-*b*-PDEA copolymers with identical PEO block length but varying PDEA block lengths (f_{EO} in the range of 0.16−0.47, see Table 1) were employed for micellization kinetic studies via stopped-flow. To directly correlate the kinetic data with the equilibrium structural parameters of self-assembled micelles, the micellar solution employed for LLS and TEM studies were prepared via pH-jump from 3 to 12 under stopped-flow mixing conditions, which can realize the pH-jump within ∼1 ms. Mezei et al.[53] recently investigated the effects of different mixing protocols on the charged nature and size distribution of hyperbranched poly(ethylene imine) (PEI)/sodium dodecyl sulfate (SDS) complexes formed in aqueous solution. It was found that at a large excess of SDS, colloidal dispersion of isolated PEI/SDS nanoparticles formed via an extremely rapid mixing of the components on a stopped-flow apparatus. However, large clusters were typically formed if a less efficient mixing protocol was chosen.

Tan et al.[35] studied the micellization of PEO_{113}-*b*-$PDEA_{70}$ in aqueous solution initially at acidic pH upon the increase of pH via dropwise addition of NaOH solution under stirring. At pH 11, micelles with an average hydrodynamic radius, $\langle R_h\rangle$, of 19.8 nm and an average aggregation number, N_{agg}, of ∼85 formed. For PEO_{113}-*b*-$PDEA_{61}$ and PEO_{113}-*b*-$PDEA_{89}$ copolymers, the micellization was realized via stopped-flow pH-jump from 3 to 12. The mixed solution was then collected for static and dynamic LLS analysis. Micelles with $\langle R_h\rangle$ of 13 and 14 nm formed for PEO_{113}-*b*-$PDEA_{61}$ and PEO_{113}-*b*-$PDEA_{89}$ copolymers, respectively, which is smaller than that reported for PEO_{113}-*b*-$PDEA_{70}$ (∼20 nm). Moreover, micelles prepared via efficient stopped-flow mixing also possessed considerably smaller N_{agg} (see Table 2).

Thus, different preparation protocols led to the formation of micelles with varying sizes and N_{agg}. This suggested that the formed aggregates were in the kinetically trapped state; however, they are stable due to the slow exchange of chains between micelles. Nyrkova and Semenov[41,42] argued that the unimer−micelle transition of block copolymers should be characterized by a continuous spectrum of relaxation times and that final equilibrium structures will never form. Recently, Cui et al.[54]

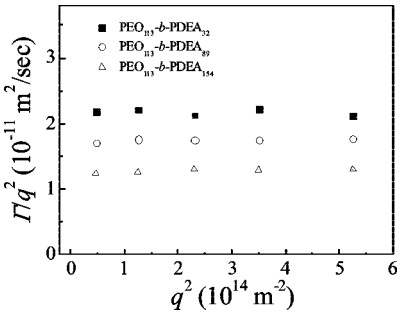

Figure 1. Variation of average characteristic line width (Γ/q^2) as a function of scattering vector (q^2) obtained for micellar solutions of PEO_{113}-*b*-$PDEA_m$ diblock copolymers prepared via stopped-flow pH-jump from 3 to 12. The final polymer concentration was at 2.0 g/L.

has utilized this property to control the block copolymer self-assembly pathways and successfully created multicompartment cylinders with phase-separated cores and cylindrical nanostructures with alternating layers of chemistry via the combination of charged block interactions with multivalent counterions and solvent mixing.

As f_{EO} was in the range of 0.16−0.47 for the five PEO-*b*-PDEA copolymers used in this study, they might form varying morphologies such as micelles, rodlike micelles, and vesicles, especially for PEO-*b*-PDEA copolymers with low f_{EO}.[19,23] Figure 1 shows the variation of average characteristic line width (Γ/q^2) as a function of scattering vector (q^2) obtained for micellar solutions of PEO_{113}-*b*-$PDEA_{32}$, PEO_{113}-*b*-$PDEA_{89}$, and PEO_{113}-*b*-$PDEA_{154}$ copolymers prepared under highly efficient stopped-flow mixing conditions upon a pH-jump from 3 to 12. We can tell that Γ/q^2 values were independent of the detection angle in all cases, suggesting the formation of spherical micelles.

Transmission electron microscopy observations were further performed on micellar solutions to examine the self-assembled morphologies. Figure 2 shows the TEM images obtained for micellar solutions of PEO_{113}-*b*-$PDEA_{117}$ and PEO_{113}-*b*-$PDEA_{154}$ copolymers, revealing the presence of spherical nanoparticles. The particle sizes were in the range of 10−20 and 15−25 nm in diameter for PEO_{113}-*b*-$PDEA_{117}$ and PEO_{113}-*b*-$PDEA_{154}$, respectively, which generally agrees with those determined from dynamic LLS (Table 2). For spherical micelles self-assembled from PEO-*b*-PDEA copolymers prepared under stopped-flow mixing conditions, they should consist of PDEA cores and PEO outer coronas due to that the PDEA block becomes water-insoluble in alkaline media.[27] As compared to that of Tan et al.[35] and Adams et al.,[19] the discrepancies in sizes and final morphologies of self-assembled aggregates of PEO-*b*-PDEA copolymers in the current study should be ascribed to the combined effects of preparation protocols and different sample PDI.

Table 2 summarized the LLS characterization results obtained for micelles of a series of PEO-*b*-PDEA copolymers (f_{EO} range, 0.16−0.47). $\langle R_h \rangle$ and N_{agg} of spherical micelles were in the range of 11−19 nm and 35−87, respectively. Each of them generally increased with increasing hydrophobic PDEA block lengths. Assuming that PEO corona of all PDEA-core micelles occupy the same brush thickness, the average radii of insoluble PDEA cores, $\langle R_c \rangle$, can be estimated from the scaling law proposed by Wu and Gao.[55] $\langle R_c \rangle$ was in the range of 2−10 nm and generally proportional to the DP of insoluble PDEA blocks. With the use of the equation $\langle \rho \rangle = M_w/(4/3\pi N_a \langle R_h \rangle^3)$, the average micelle density, $\langle \rho \rangle$, of PEO-*b*-PDEA copolymers micelles was estimated to be in the range of 0.12−0.18 g/cm^3. The relatively low average density of micelles might reflect that the PEO corona was highly swollen.

The above LLS and TEM results of micelles prepared under efficient mixing conditions can be directly used to correlate with subsequent stopped-flow micellization kinetic studies. The main difference between these techniques is that the former two mainly characterize the structures of final aggregates, whereas the stopped-flow technique can monitor the kinetic aspects during micellization. As the self-assembled aggregates might be in a kinetically trapped state, understanding the unimer-to-micelle transition kinetics would play a crucial role in elucidating the kinetic sequences and controlling the morphology and structure of the final aggregates.

Stopped-Flow Kinetics. Figure 3 shows time-dependent scattered intensity obtained for aqueous solutions of PEO_{113}-*b*-$PDEA_{154}$ copolymer upon pH-jump from 3 to various final pH values. At a final pH < 6, the relaxation curve remains a straight line; the diblock copolymer chains still exist as unimers. In the final pH range of 6.7−7.2, kinetic traces with negative amplitudes were observed, indicating the possible formation of loose aggregates.[35]

At a final pH ≥ 7.7, relaxation processes with quite large positive amplitudes can be typically observed. The time dependence of the scattered light intensity I_t can be converted to a normalized function, namely, $(I_\infty - I_t)/I_\infty$ versus t, where I_∞ is the value of I_t at an infinitely long time. It was found that single exponential function can not fit the relaxation curve (Figure 4a), especially for the first 0.2 s. However, the dynamic trace can be well-fitted by a double exponential function (Figure 4b):

$$(I_\infty - I_t)/I_\infty = c_1 e^{-t/1} + c_2 e^{-t/2} \quad (2)$$

where c_1 and c_2 are the normalized amplitudes ($c_2 = 1 - c_1$) and τ_1 and τ_2 are the characteristic relaxation time of two processes, $\tau_1 < \tau_2$. The mean relaxation time for the overall micelle formation, τ_f, can be calculated as

$$\tau_f = c_1\tau_1 + c_2\tau_2 \quad (3)$$

Both τ_1 and τ_2 have positive amplitudes. Upon the pH-jump from 3 to 12 at a final copolymer concentration of 2.0 g/L, τ_1 and τ_2 are 13 and 171 ms, respectively. The calculated τ_f based on eq 3 is 43 ms. Following similar principles employed previously, τ_1 can be assigned to the rapid association of unimers into quasi-equilibrium micelles, whereas τ_2 can be ascribed to the relaxation of quasi-equilibrium micelles into final stable aggregates via micelle formation/breakup.

Figure 5 shows the time-dependent scattered intensity obtained for the aqueous solution of PEO_{113}-*b*-$PDEA_{154}$ copolymer upon a pH-jump from 3 to 12 at different final concentrations. The corresponding double exponential fitting results are shown in Figure 6. The characteristic relaxation times τ_1 decreases with increasing copolymer concentrations. This strongly suggests that relaxation from initially formed transient micelles to quasi-equilibrium micelles mainly proceeds via micelle fusion/fission. For the relaxation from quasi-equilibrium micelles to the final stable aggregates, τ_2 also decreases with increasing copolymer concentrations, suggesting that the micelle fusion/fission mechanism also dominates in the second slow process.[40]

Figure 7 shows the concentration dependence of τ_2 obtained from double exponential fitting of dynamic traces recorded for aqueous solutions of all five PEO-*b*-PDEA copolymers with varying PDEA chain lengths upon a stopped-flow pH-jump from 3 to 12. Interestingly, we can observe that for PEO_{113}-*b*-$PDEA_{32}$ and PEO_{113}-*b*-$PDEA_{61}$, τ_2 are almost independent of polymer

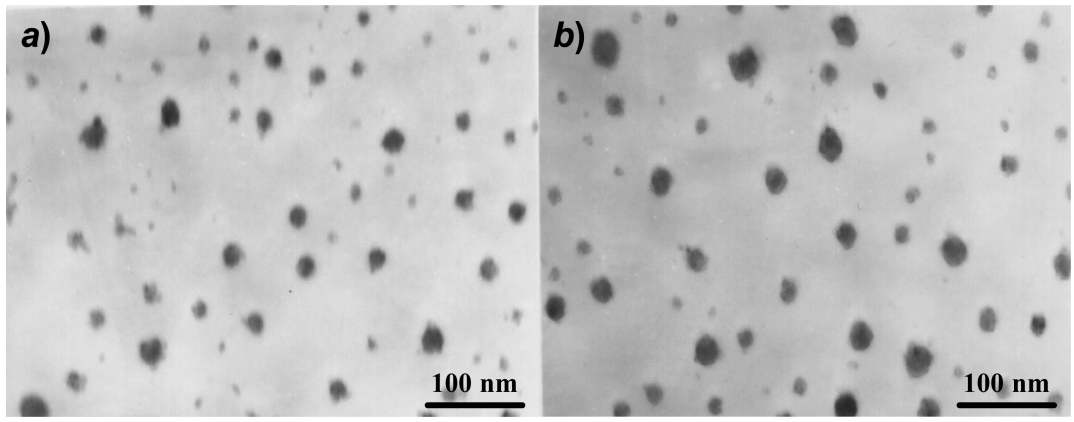

Figure 2. Typical transmission electron microscopy (TEM) images obtained for micellar solutions of (a) PEO_{113}-*b*-$PDEA_{117}$ and (b) PEO_{113}-*b*-$PDEA_{154}$ copolymers prepared via stopped-flow pH-jump from 3 to 12.

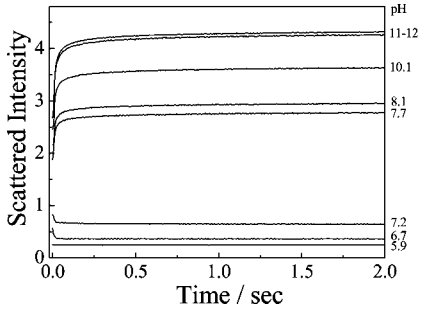

Figure 3. Time dependence of scattered light intensity obtained for aqueous solutions of PEO_{113}-*b*-$PDEA_{154}$ copolymer upon a stopped-flow pH-jump from 3 to various final pH values. The final copolymer concentration was fixed at 2.0 g/L.

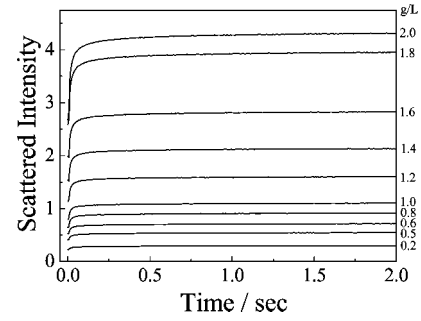

Figure 5. Time dependence of scattered light intensity obtained for aqueous solutions of PEO_{113}-*b*-$PDEA_{154}$ diblock copolymer upon a pH-jump from 3 to 12. The final copolymer concentrations (g/L) were varied.

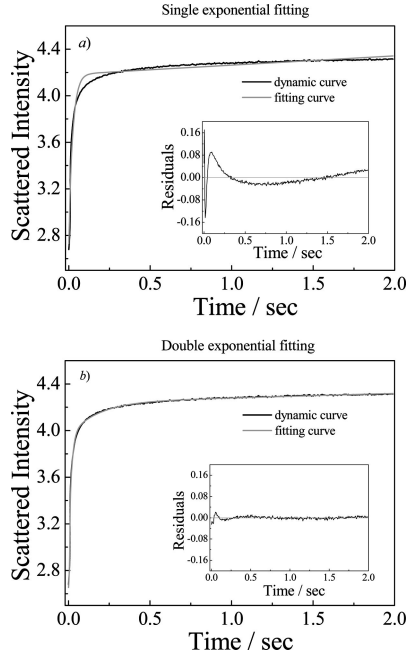

Figure 4. (a) Single and (b) double exponential fitting of dynamic traces obtained for aqueous solutions of PEO_{113}-*b*-$PDEA_{154}$ diblock copolymer upon a stopped-flow pH-jump from 3 to 12. The final copolymer concentration was 2.0 g/L.

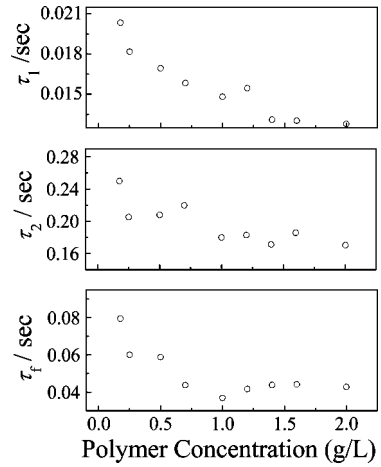

Figure 6. Double exponential fitting results of dynamic traces shown in Figure 5. The experimental conditions were the same as those described in Figure 5.

concentrations, remaining constant at ~300 and 200 ms, respectively. This suggests that the relaxation from quasi-equilibrium micelles into final stable ones mainly proceeds via insertion/expulsion of unimer chains. On the other hand, upon increasing the PDEA block lengths to 89, 117, and 154, the obtained τ_2, generally tends to decrease with increasing polymer concentration, indicating that the micelle fusion/fission mechanism dominates in the second slow process.

The observed concentration independence of τ_2 for PEO_{113}-*b*-$PDEA_{32}$ and PEO_{113}-*b*-$PDEA_{61}$ can be rationalized as follows. At the beginning of the second slow process, unimer concentration is already close to the critical micellization concentration (cmc). The subsequent micelle growth process will involve the decomposition of initially formed quasi-equilibrium micelles. This disintegration process is actually the rate-determining step, and thus the slow process exhibits no polymer concentration dependence.

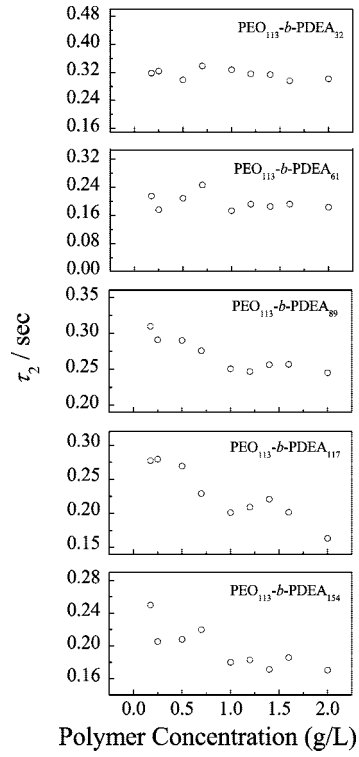

Figure 7. Concentration dependence of τ_2 obtained from double exponential fitting of dynamic traces recorded for aqueous solutions of PEO_{113}-*b*-$PDEA_m$ copolymers (listed in Table 1) upon a stopped-flow pH-jump from 3 to 12.

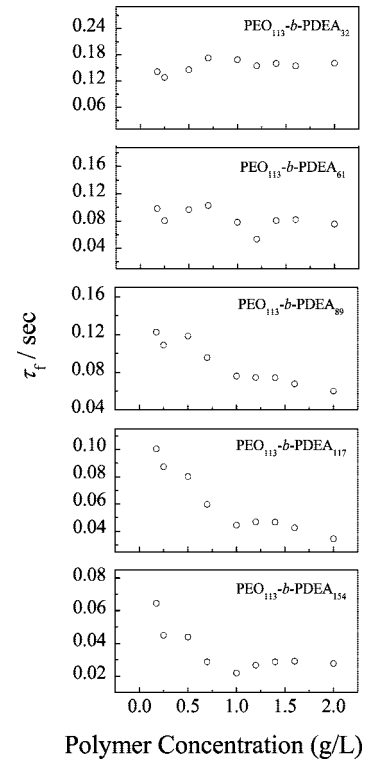

Figure 8. Concentration dependence of τ_f obtained from double exponential fitting of dynamic traces recorded for aqueous solutions of PEO_{113}-*b*-$PDEA_m$ diblock copolymer upon a stopped-flow pH-jump from 3 to 12.

Dormidontova[40] proposed that during the slow process, unimer insertion into existing micelles might contain two consecutive steps, namely, the penetration into micelle corona and subsequently into micelle core. Both characteristic relaxation times, τ_{corona} and τ_{core}, will exponentially increase with the increase of hydrophobic block length. On the other hand, the micelle fusion process contains three sequential steps: micelle diffusion, "deformation" of micelle coronas (i.e., the time for cores of neighboring micelles to come into contact), and merging of micelle cores. The relaxation time of first two steps is dependent on the hydrophilic block length but relatively independent of the hydrophobic block length.

Thus, compared to that of the substeps associated with micelle fusion/fission process, the exponential increase of relaxation time with hydrophobic block length for the unimer insertion/expulsion process (if involved) can well explain the transformation of mechanism into micelle fusion/fission for copolymers with larger hydrophobic PDEA block lengths during their micellization. Furthermore, if unimer insertion/expulsion mechanism is dominant for all five copolymers, it is expected that the whole micellization process will be much slower with the increase of PDEA chain lengths, because micelles with larger N_{agg} will eventually form (Table 2). This is contrary to the results shown in Figure 8, from which we can clearly see that the micellization is actually getting considerably faster for copolymers with increasing PDEA chain lengths at comparable polymer concentrations. Intuitively, the increase of hydrophobic chain lengths provides larger driving force for the micellization, leading to faster self-assembly kinetics. Finally, chain entanglement within the micelle core might develop during micellization, which is especially true for copolymers with larger PDEA block lengths. This will provide additional energy barriers for the unimer insertion/expulsion process. Thus, during the micellization of PEO-*b*-PDEA copolymer with longer PDEA (DP ≥ 89), micelle fusion/fission mechanism dominates during the second slow process, i.e., this mechanism provides faster micelle relaxation pathways.

Wu[56] has proposed a simple model for the structure of microemulsion droplets and suggested that, for a given dispersion, the particle surface area occupied per stabilizer is close to a constant. A reanalysis of the structural parameters (Table 2) of micelles self-assembled from five PEO-*b*-PDEA copolymers indicates that the surface area per PEO stabilizing block at the surface of micelle corona fluctuates around ~50 nm^2. This indicates that for both relaxation pathways, namely, unimer insertion/expulsion and micelle fusion/fission, micellization of PEO-*b*-PDEA copolymers with shorter and longer PDEA block lengths will eventually lead to the formation of final stable aggregates.

Different micelle relaxation pathways should possess characteristically distinct activation energies.[57] Figure 9 shows Arrhenius plots of τ_2 obtained from double exponential fitting of dynamic traces recorded for aqueous solutions of a series of PEO-*b*-PDEA copolymers upon a stopped-flow pH-jump from 3 to 12. It is quite expected that in all cases, τ_2 decreases with increasing temperature as observed for conventional surfactants.[58] Arrhenius plots in Figure 9 yield apparent activation energies of 6.81, 8.05, 3.87, 3.34, and 3.10 kJ/mol for the slow process (τ_2) during the micellization of PEO_{113}-*b*-$PDEA_{32}$, PEO_{113}-*b*-$PDEA_{61}$, PEO_{113}-*b*-$PDEA_{89}$, PEO_{113}-*b*-$PDEA_{117}$, and PEO_{113}-*b*-$PDEA_{154}$ copolymers, respectively. For the relaxation of small molecule surfactant micelles, it has been established that the activation energy for the micelle formation/breakup via stepwise unimer association/dissociation is much larger than that via micelle fusion/fission.[59] For PEO_{113}-*b*-$PDEA_{89}$, PEO_{113}-*b*-$PDEA_{117}$, and PEO_{113}-*b*-$PDEA_{154}$ copolymers, they exhibit considerably lower E_a compared to those obtained for PEO_{113}-*b*-$PDEA_{32}$ and PEO_{113}-*b*-$PDEA_{61}$ copolymer. This suggests that

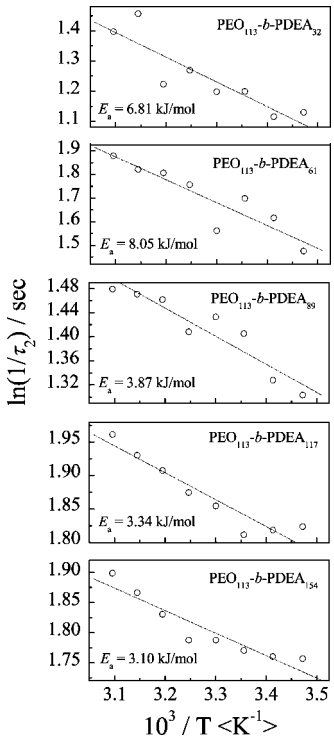

Figure 9. Arrhenius plots of τ_2 obtained from double exponential fitting of dynamic traces recorded for aqueous solutions of PEO_{113}-*b*-$PDEA_m$ copolymers upon a stopped-flow pH-jump from 3 to 12 at different temperatures. The final copolymer concentration was fixed at 2.0 g/L.

PEO-*b*-PDEA copolymers with varying hydrophobic PDEA blocks follow different relaxation pathways during the micellization process.

Conclusion

In order to elucidate the hydrophobic chain-length effects on the unimer-to-micelle transition kinetics, we synthesized a series of well-defined poly(ethylene oxide)-*b*-poly(2-(diethylamino)-ethyl methacrylate), PEO-*b*-PDEA, diblock copolymers containing identical PEO block and PDEA block with varying DPs (in the range of 32−154), and their pH-induced micellization kinetics were recorded employing the stopped-flow technique. For PEO_{113}-*b*-$PDEA_{32}$ and PEO_{113}-*b*-$PDEA_{61}$ copolymers, unimer insertion/expulsion mechanism mainly dominated the relaxation from quasi-equilibrium micelles into final stable micelles, i.e., the second slow process associated with micelle formation/breakup, during micellization. Upon increasing the DP of pH-responsive PDEA block to 89, 117, and 154, the slow process was found to be dominated by the micelle fusion/fission mechanism. Moreover, the mechanism transformation upon increasing the DP of PDEA block was further confirmed by temperature-dependent micellization kinetic studies, revealing that copolymers with longer PDEA blocks possessed considerably lower apparent activation energy (E_a) compared to those with shorter ones. To the best of our knowledge, this represented the first experimental study to probe the hydrophobic chain-length dependence of unimer-to-micelle transition kinetics, and the mechanism transformation during micellization of block copolymers with increasing hydrophobic chain lengths was unprecedented.

Acknowledgment. The financial supports of the National Natural Scientific Foundation of China (NNSFC) Projects 20534020, 20674079, and 50425310, Specialized Research Fund for the Doctoral Program of Higher Education (SRFDP), and the Program for Changjiang Scholars and Innovative Research Team in University (PCSIRT) are gratefully acknowledged.

References and Notes

(1) Colfen, H. *Macromol. Rapid Commun.* **2001**, *22*, 219–252.
(2) Rodriguez-Hernandez, J.; Lecommandoux, S. *J. Am. Chem. Soc.* **2005**, *127*, 2026–2027.
(3) Virtanen, J.; Arotcarena, M.; Heise, B.; Ishaya, S.; Laschewsky, A.; Tenhu, H. *Langmuir* **2002**, *18*, 5360–5365.
(4) Andre, X.; Zhang, M. F.; Muller, A. H. E. *Macromol. Rapid Commun.* **2005**, *26*, 558–563.
(5) Dai, S.; Ravi, P.; Tam, K. C.; Mao, B. W.; Gang, L. H. *Langmuir* **2003**, *19*, 5175–5177.
(6) Butun, V.; Liu, S.; Weaver, J. V. M.; Bories-Azeau, X.; Cai, Y.; Armes, S. P. *React. Funct. Polym.* **2006**, *66*, 157–165.
(7) Poe, G. D.; McCormick, C. L. *J. Polym. Sci., Part A: Polym. Chem.* **2004**, *42*, 2520–2533.
(8) Gohy, J. F. *Adv. Polym. Sci.* **2005**, *190*, 65–136.
(9) Riess, G. *Prog. Polym. Sci.* **2003**, *28*, 1107–1170.
(10) Li, Y.; Lokitz, B. S.; McCormick, C. L. *Angew. Chem., Int. Ed.* **2006**, *45*, 5792–5795.
(11) Alarcon, C. D. H.; Pennadam, S.; Alexander, C. *Chem. Soc. Rev.* **2005**, *34*, 276–285.
(12) Cunliffe, D.; Alarcon, C. D.; Peters, V.; Smith, J. R.; Alexander, C. *Langmuir* **2003**, *19*, 2888–2899.
(13) Hoffmann, J.; Plotner, M.; Kuckling, D.; Fischer, W. J. *Sens. Actuators, A* **1999**, *77*, 139–144.
(14) Ista, L. K.; Lopez, G. P. *J. Ind. Microbiol. Biotechnol.* **1998**, *20*, 121–125.
(15) Kim, S. J.; Park, S. J.; Lee, S. M.; Lee, Y. M.; Kim, H. C.; Kim, S. I. *J. Appl. Polym. Sci.* **2003**, *89*, 890–894.
(16) Nandkumar, M. A.; Yamato, M.; Kushida, A.; Konno, C.; Hirose, M.; Kikuchi, A.; Okano, T. *Biomaterials* **2002**, *23*, 1121–1130.
(17) Rodriguez-Hernandez, J.; Checot, F.; Gnanou, Y.; Lecommandoux, S. *Prog. Polym. Sci.* **2005**, *30*, 691–724.
(18) Yamato, M.; Utsumi, M.; Kushida, A.; Konno, C.; Kikuchi, A.; Okano, T. *Tissue Eng.* **2001**, *7*, 473–480.
(19) Adams, D. J.; Butler, M. F.; Weaver, A. C. *Langmuir* **2006**, *22*, 4534–4540.
(20) Cai, Y. L.; Armes, S. P. *Macromolecules* **2004**, *37*, 7116–7122.
(21) Narain, R.; Armes, S. P. *Biomacromolecules* **2003**, *4*, 1746–1758.
(22) Zhang, W.; Shi, L.; Wu, K.; An, Y. *Macromolecules* **2005**, *38*, 5743–5747.
(23) Won, Y. Y.; Brannan, A. K.; Davis, H. T.; Bates, F. S. *J. Phys. Chem. B* **2002**, *106*, 3354–3364.
(24) Chen, G. P.; Ito, Y.; Imanishi, Y. *Macromolecules* **1997**, *30*, 7001–7003.
(25) Martin, T. J.; Prochazka, K.; Munk, P.; Webber, S. E. *Macromolecules* **1996**, *29*, 6071–6073.
(26) Amalvy, J. I.; Wanless, E. J.; Li, Y.; Michailidou, V.; Armes, S. P.; Duccini, Y. *Langmuir* **2004**, *20*, 8992–8999.
(27) Webber, G. B.; Wanless, E. J.; Butun, V.; Armes, S. P.; Biggs, S. *Nano Lett.* **2002**, *2*, 1307–1313.
(28) Liu, S. Y.; Weaver, J. V. M.; Tang, Y. Q.; Billingham, N. C.; Armes, S. P.; Tribe, K. *Macromolecules* **2002**, *35*, 6121–6131.
(29) Butun, V.; Armes, S. P.; Billingham, N. C. *Polymer* **2001**, *42*, 5993–6008.
(30) Butun, V.; Armes, S. P.; Billingham, N. C. *Macromolecules* **2001**, *34*, 1148–1159.
(31) Butun, V.; Liu, S.; Weaver, J. V. M.; Bories-Azeau, X.; Cai, Y.; Armes, S. P. *React. Funct. Polym.* **2006**, *66*, 157–165.
(32) Liu, S. Y.; Billingham, N. C.; Armes, S. P. *Angew. Chem., Int. Ed.* **2001**, *40*, 2328.
(33) Weaver, J. V. M.; Armes, S. P.; Butun, V. *Chem. Commun.* **2002**, *2122*, 2123.
(34) Lee, A. S.; Butun, V.; Vamvakaki, M.; Armes, S. P.; Pople, J. A.; Gast, A. P. *Macromolecules* **2002**, *35*, 8540–8551.
(35) Tan, J. F.; Ravi, P.; Too, H. P.; Hatton, T. A.; Tam, K. C. *Biomacromolecules* **2005**, *6*, 498–506.
(36) Weaver, J. V. M.; Armes, S. P.; Liu, S. *Macromolecules* **2003**, *36*, 9994–9998.
(37) Wang, Y. M.; Mattice, W. L.; Napper, D. H. *Langmuir* **1993**, *9*, 66–70.
(38) Esselink, F. J.; Dormidontova, E. E.; Hadziioannou, G. *Macromolecules* **1998**, *31*, 4873–4878.
(39) Esselink, F. J.; Dormidontova, E.; Hadziioannou, G. *Macromolecules* **1998**, *31*, 2925–2932.
(40) Dormidontova, E. E. *Macromolecules* **1999**, *32*, 7630–7644.

(41) Nyrkova, I. A.; Semenov, A. N. *Macromol. Theory Simul.* **2005**, *14*, 569–585.
(42) Nyrkova, I. A.; Semenov, A. N. *Faraday Discuss.* **2005**, *128*, 113–127.
(43) Zhu, Z. Y.; Armes, S. P.; Liu, S. Y. *Macromolecules* **2005**, *38*, 9803–9812.
(44) Zhu, Z.; Xu, J.; Zhou, Y.; Jiang, X.; Armes, S. P.; Liu, S. *Macromolecules* **2007**, *40*, 6393–6400.
(45) Tan, J. F.; Hatton, T. A.; Tam, K. C.; Too, H. P. *Biomacromolecules* **2007**, *8*, 448–454.
(46) Vamvakaki, M.; Billingham, N. C.; Armes, S. P. *Macromolecules* **1999**, *32*, 2088–2090.
(47) Matyjaszewski, K.; Wei, M. L.; Xia, J. H.; McDermott, N. E. *Macromolecules* **1997**, *30*, 8161–8164.
(48) Xia, J. H.; Matyjaszewski, K. *Macromolecules* **1997**, *30*, 7697–7700.
(49) Bories-Azeau, X.; Armes, S. P. *Macromolecules* **2002**, *35*, 10241–10243.
(50) Jiang, Y.; Chen, T.; Ye, F.; Liang, H.; Shi, A. C. *Macromolecules* **2005**, *38*, 6710–6717.
(51) Terreau, O.; Bartels, C.; Eisenberg, A. *Langmuir* **2004**, *20*, 637–645.
(52) Terreau, O.; Luo, L.; Eisenberg, A. *Langmuir* **2003**, *19*, 5601–5607.
(53) Mezei, A.; Meszaros, R.; Varga, I.; Gilanyi, T. *Langmuir* **2007**, *23*, 4237–4247.
(54) Cui, H. G.; Chen, Z. Y.; Zhong, S.; Wooley, K. L.; Pochan, D. J. *Science* **2007**, *317*, 647–650.
(55) Wu, C.; Gao, J. *Macromolecules* **2000**, *33*, 645–646.
(56) Wu, C. *Macromolecules* **1994**, *27*, 298–299.
(57) Michels, B.; Waton, G.; Zana, R. *Langmuir* **1997**, *13*, 3111–3118.
(58) Aniansson, E. A. G.; Wall, S. N. *J. Phys. Chem.* **1975**, *79*, 857–858.
(59) Tondre, C.; Zana, R. *J. Colloid Interface Sci.* **1978**, *66*, 544.

JP803700N